

Cite this: *RSC Adv.*, 2017, **7**, 30879

Supercritical CO₂ dried chitosan nanoparticles: production and characterization

F. J. Caro León,^a J. Lizardi-Mendoza,^{id *a} W. Argüelles-Monal,^{id b} E. Carvajal-Millan,^{id a} Y. L. López Franco^{id a} and F. M. Goycoolea^{id c}

Herein are reported the production and characteristics of chitosan nanoparticles that go through supercritical CO₂ drying. First, chitosan nanoparticles in aqueous colloidal suspension were produced by ionic crosslinking with sodium tripolyphosphate. The produced nanoparticles have a surface charge (ζ -potential) of +27 mV and an average diameter of approximately 100 nm, measured by dynamic light scattering and field emission-scanning electron microscopy observations. The liquid phase of the nanoparticle suspension was replaced successively with ethanol and supercritical CO₂ to produce dried chitosan nanoparticles finally. The main characteristics of the obtained nanoparticles were determined by diverse analytical techniques. Infrared spectroscopy, solid-state ¹³C nuclear magnetic resonance and X-ray diffraction studies were performed to explore possible physicochemical changes induced by the drying procedure. Also, the thermal stability of the dry chitosan nanoparticles was determined by thermogravimetric assay and dynamic scanning calorimetry. Structural properties were analyzed and compared with lyophilized nanoparticles finding that the supercritically dried chitosan nanoparticles have a surface area an order of magnitude higher. Microscopy images showed that the supercritically dried chitosan nanoparticles have a porous conglomerated structure, suggesting that there is particle aggregation through the drying process. Notwithstanding, the dry chitosan nanoparticles resuspended in the dilute acid medium readily; microscopy observations showed that the size of the resuspended particles remains in the nanoscale range. The proposed procedure is able to furnish dried chitosan nanoparticles with structural characteristics and functional properties that are appealing for their use in diverse applications.

Received 1st March 2017

Accepted 8th June 2017

DOI: 10.1039/c7ra02555f

rsc.li/rsc-advances

1. Introduction

Polysaccharides are natural compounds that have been proved valuable for application in diverse areas mainly due to their structural properties, stability and biocompatibility.¹ Chitosan (Cs) is a linear aminopolysaccharide composed of 2-acetamide-2-deoxy-D-glucopyranose and 2-amino-2-deoxy-D-glucopyranose (*N*-acetyl glucosamine and glucosamine units, respectively) linked by $\beta(1 \rightarrow 4)$ bonds. The amino groups distributed along the Cs chain provide it with a polycationic character, a rather unique feature among natural polymers. The attention to this biopolymer has been increasing over the years due to its availability and a set of interesting functional properties, including being biocompatible, biodegradable, non-toxic, antimicrobial, adsorptive, mucoadhesive, hemostatic, among others.²⁻⁴ Since

the chemical characteristics of Cs, particularly the molecular weight and degree of acetylation, determine such functional properties it is possible to choose or adjust them according to the application.⁵⁻⁷ Consequently, chitosan is one of the biopolymers most extensively used to a wide range of materials such as films, gels, scaffolds, capsules or particulates.⁸⁻¹²

The use of biopolymers, particularly chitosan, in nanotechnology began exploring biocompatible alternatives to metals, inorganic compounds and synthetic polymers that provide limited stability to incorporated proteins.¹³ Initially, Cs nanoparticles were obtained generating covalent bonds between the amino groups of the polysaccharide with diverse cross-linking agents (e.g. glutaraldehyde).^{14,15} Later, Cs nanoparticles based on ionic interactions were developed to avoid the use of potentially toxic solvents, cross-linkers or other additives.^{16,17} Further research explores the utility of physical interactions for simplified preparation of Cs nanoparticles.¹⁸ Over the years, different preparation processes have been proposed trying to improve the properties of the nanoparticulated systems such as size, stability, surface charge and drug loading capacity.^{13,14}

The use of nanoparticles in colloidal suspensions faces several difficulties imposed by instability processes that could be of physical (*i.e.* aggregation or sedimentation) or chemical

^aCentro de Investigación en Alimentación y Desarrollo A.C., Grupo de Investigación en Biopolímeros, Carr. a La Victoria km 0.6, Hermosillo, Sonora, Mexico, 83304. E-mail: jalm@ciad.mx

^bCentro de Investigación en Alimentación y Desarrollo A.C., Coord. Reg. Guaymas, Polímeros Naturales, Carr. a Varadero Nacional km. 6.6, Guaymas, Sonora, Mexico, 85480

^cSchool of Food Science and Nutrition, University of Leeds, Woodhouse Ln, Leeds LS2 9JT, UK



nature (*i.e.* hydrolysis, diffusion or reactivity). The occurrence of these problems is reflected in the limited time that nanoparticle suspensions may be stored.¹⁹ Removing the liquid phase, usually water, from the colloidal suspension is an effective way to improve the stability of the nanoparticles. Furthermore, dry nanoparticles are usually preferred in certain applications, such as drug delivery formulation for inhalation.²⁰ The most used procedures to obtain dry chitosan nanoparticles either rely on evaporation (*e.g.* spray-drying) or sublimation (*e.g.* freeze-drying) to remove water or other solvents.^{19,21}

The supercritical CO_2 (sc CO_2) technology provides alternatives to produce diverse nanoparticles.²² However, the production of chitosan nanoparticles from aqueous solutions is mainly constrained by the low solubility of water in sc CO_2 . Up to this point, some supercritical techniques depending on compatible co-solvents and specially configured equipment (*e.g.* supercritical anti-solvent, supercritical assisted atomization or rapid expansion of supercritical solution) have been used to obtain nanoparticles containing chitosan.^{23–26} Although there are reports about the use of simple sc CO_2 drying procedures to obtain Cs materials with different sizes and morphologies, such as monolith and microparticles,^{27,28} none of these materials is at the nanoscale. Usually, the materials obtained by sc CO_2 drying have the large specific surface area, low density and mesoporous structure, providing appealing properties for diverse applications, including active transport of bioactive substances.^{29–32} As a result, sc CO_2 drying was used to process Cs nanoparticles previously produced by ionotropic gelation. The physicochemical and structural properties of the dry Cs nanoparticles were studied and reported. The performance of the dry Cs nanoparticles on resuspension and the comparison with freeze dried Cs nanoparticles were also analyzed.

2. Experimental

The materials used and experimental procedures are described below. Also, the experimental scheme is included in Fig. 1.

2.1. Materials

Chitosan was provided by Primex (ChitoClear); it has a degree of acetylation (DA) of 20% and weight average molecular mass (M_w) of 250 kg mol^{−1} (supplier data). Tripolyphosphate

pentasodium salt (TPP) practical grade was obtained from Sigma-Aldrich (St. Louis, Missouri, USA). Reagent grade solvents and chemicals, acquired from recognized commercial distributors, were used. Deionized water was utilized throughout unless stated otherwise.

2.2. Nanoparticle preparation and characterization

An aqueous suspension of Cs nanoparticles (CsN) was produced by previously described ionotropic gelation method with some modifications.³³ Briefly, Cs was fully dissolved (1.0 mg mL^{−1}) in 2% v/v CH_3COOH under magnetic stirring. The pH of the solution was adjusted to 6.1 with NaOH (6% w/w). The nanoparticles were spontaneously formed upon mixing 20 mL of a TPP solution (1.0 mg mL^{−1}) into 30 mL of the Cs solution under magnetic stirring (~400 rpm) at room temperature for 10 min. The size of the nanoparticles was determined by dynamic light scattering with a non-invasive back scattering (DLS/NIBS) technology; simultaneously, the zeta potential (ζ -potential) of the particles was determined by laser Doppler electrophoresis with phase analysis light scattering (M3-PALS) using a Zetasizer Nano-ZS (ZEN 3600, Malvern instruments, Worcestershire, UK). The morphology of the CsN was studied by field emission-scanning electron microscopy (FE-SEM) using a SU 8000 Hitachi microscopy. To this end, 10 μL of nanoparticles suspension was dropped on a copper grid coated with a Formvar membrane, allowed to stand for 5 minutes, dried, and coated with Au/Pd.

2.3. Nanoparticle drying

The CsN were subjected to sc CO_2 drying as follows. First, the aqueous medium of the nanoparticles was replaced with ethanol transferring the nanoparticles to 25, 50, 75 and 100% ethanol successively. Then, the ethanol was exchanged with CO_2 in supercritical conditions in a pressurized vessel (74 bar, 45 °C). Finally, the CO_2 was slowly released leaving dry Cs nanoparticles (DCsN).

2.4. Physicochemical characterization

The main characteristics of the pristine Cs and the DCsN were determined using several techniques. Solid-state cross-polarization magic angle spinning ^{13}C nuclear magnetic

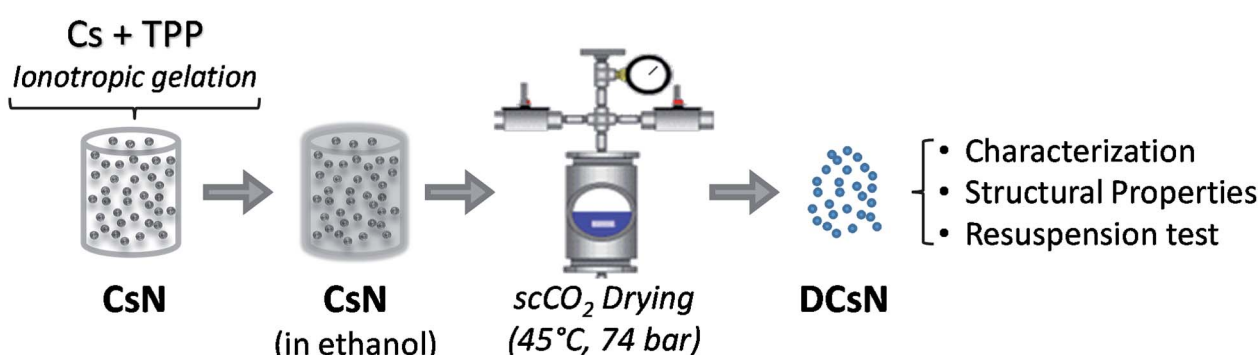


Fig. 1 Experimental scheme for dry Cs nanoparticles production and characterization.

resonance (CP/MAS ^{13}C -NMR) was performed in a Bruker Avance TM 400WB equipped with a wide-mouth superconducting magnet (89 mm) operating at 9.4 tesla. The experimental conditions were: 4.4 μs width 90° pulse with 4 s repetition time, cross-polarization contact time of 1 ms and spectra accumulation of 2000 scans, the samples were contained in a cylindrical ceramic rotor. Attenuated total reflection Fourier transform infrared (ATR-FTIR) spectra were collected on a Perkin-Elmer Spectrum One spectrophotometer; using 64 co-added scans with 4 cm^{-1} resolution over a spectral range of 500–4000 cm^{-1} . Thermogravimetric analysis (TGA) was performed on a Q500 thermogravimetric analyzer (TA instruments), heating from 20 °C up to 800 °C at 10 °C min^{-1} rate, under nitrogen flow. Differential scanning calorimetry (DSC) was performed on DSC 7 calorimeter (Perkin Elmer) with two heating runs, first from –30 °C up to 190 °C and the second one from –30 °C up to 400 °C. X-ray diffraction (XRD) experiments were carried out on a Bruker D8 Advance diffractometer equipped with Cu $\text{K}\alpha$ radiation. The angle range (2θ) was scanned from 2° to 40° at a step size of 0.02° and the working voltage, and current were 45 kV and 100 mH, respectively. The crystallinity index (CrI) was calculated from the corresponding XRD diffractogram using the following formula:

$$\text{CrI} (\%) = \frac{(I_{110} - I_{\text{am}}) \times 100}{I_{110}}$$

where I_{110} is the maximum intensity of the 110 plane at $2\theta = 20^\circ$, and I_{am} is the intensity of the amorphous diffraction at $2\theta = 16^\circ$.³⁴

2.5. Structural characterization

Specific surface area of dried nanoparticles was determined by nitrogen sorption on a Monosorb Surface Area Analyser MS-13 (Quantachrome). The samples were degassed at 80 °C for 18 h under vacuum prior to analysis. Six points in the range of relative pressure (P/P_0) from 0.05 to 0.3 were used to calculate the surface areas by Brunauer–Emmett–Teller (BET) method.

2.6. Resuspension tests

A sample of DCsN was resuspended (0.5 mg mL^{-1}) in 2% v/v CH_3COOH under constant vigorous magnetic stirring. Size and ζ -potential of the systems were measured by DLS, and morphological study of FE-SEM was performed as described previously.

3. Results and discussion

3.1. Cs nanoparticles preparation and characterization

Under suitable conditions (e.g. Cs characteristics, reagents concentration, pH, temperature, stirring, etc.) the addition of TPP to a Cs solution produces nanoparticles due to the interaction of the positively charged polymer chains and the negatively charged TPP molecules.¹⁷ The use of TPP as chitosan crosslinker is a reliable method to produce stable nanoparticles in relatively large quantities, minimizing safety concerns. This method has been commonly used to obtain Cs nanoparticles achieving lower particle size of about 100 nm and positive ζ -

potential.^{33,35,36} In accordance with this, the size of the CsN, measured by DLS, was 97 ± 46 nm with a polydispersity index (PDI) of 0.23, and ζ -potential of $+27 \pm 4$ mV. The positive surface charge of the nanoparticles is related to the portion of amino groups of Cs not linked with TPP.³⁶ Apparently, the CsN have a spherical shape and smooth surface, as can be observed on the FE-SEM image (Fig. 2). From measurements on micrographs, the diameter of the particles is in a range of 70 to 180 nm (average 117 ± 42 nm, PDI 0.36, $n = 40$), which is congruent with the DLS data, taking into account the variance associated to these measurements. The particles that were processed by scCO_2 drying were similar to those previously reported in the literature.

3.2. DCsN characteristics

The obtained DCsN were subjected to diverse analytical techniques in order to investigate the possible physicochemical and structural changes that the drying process could induce in the material.

3.2.1. CP/MAS ^{13}C -NMR. The CP/MAS ^{13}C -NMR spectra of CS and DCsN are shown in Fig. 3. The Cs spectrum has five bands, at 57.6, 60.9, 76.1, 84 and 105.7 ppm, that correspond to the pyranose rings carbon atoms (C_2 , C_6 , $\text{C}_5 + \text{C}_3$, C_4 , C_1 ; respectively).³⁷ Additionally, the methyl and carbonyl carbons of the acetyl group of the *N*-acetyl-glucosamine units remaining in Cs correspond to the bands at 23 and 178 ppm, respectively. In the literature, similar signals display has been associated to the “tendon” polymorph of Cs.³⁸ Compared to the Cs, the DCsN spectrum shows similar peaks but broader and with lower resolution. This could be related to the layout of Cs chains and TPP molecules forming amorphous structures in the nanoparticles that induce anisotropic effects which the experimental conditions were not able to overcome.

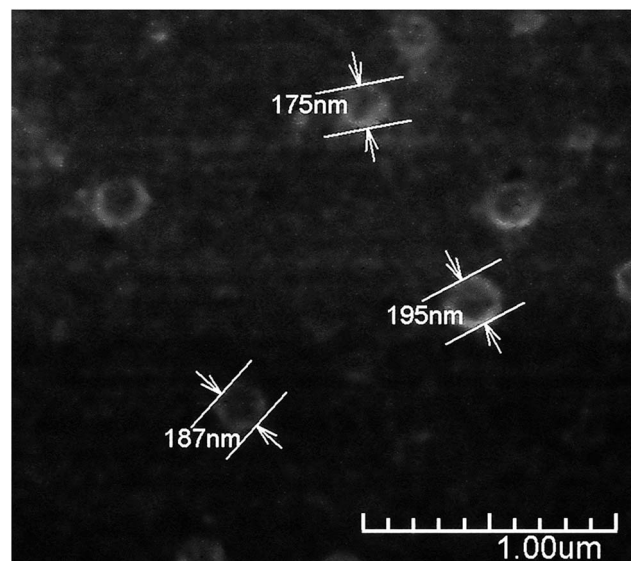
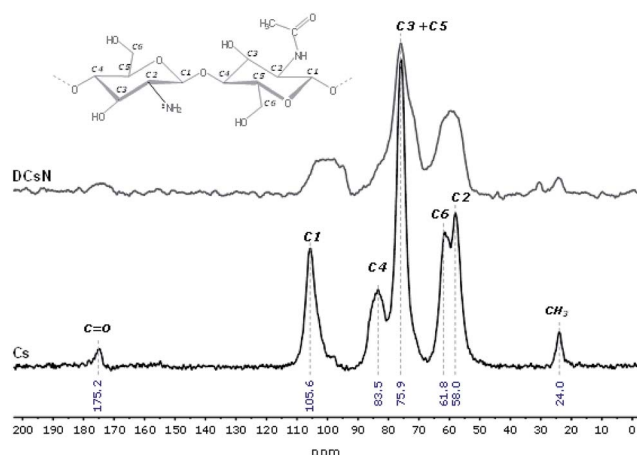


Fig. 2 FE-SEM image of the CsN. Magnification of 30 000 \times , SE detector, 1.5 kV.



Fig. 3 CP/MAS ^{13}C -NMR spectra of Cs and DCsN.

3.2.2. ATR-FTIR. The information about the chemical identity of the components of the DCsN is complemented with infrared absorption analysis. Fig. 4 includes the ATR-FTIR spectra of Cs, TPP and DCsN. For Cs, the main bands observed are centered at 3355, 2875, 1650, 1584, 1417, 1375, 1316 cm^{-1} and several overlapped bands in the fingerprint region ($1200\text{--}850\text{ cm}^{-1}$). This pattern coincides with the known infrared absorption spectrum for Cs.³⁹ By comparison, several changes are observed in the DCsN spectra. At first, the bands corresponding to the O-H and N-H stretching vibrations (3350 and 2875 cm^{-1} , respectively) become broader indicating that such bonds are involved in a larger variety of chemical environments, including multiple hydrogen bonding that could be induced by the ionic crosslinking between Cs and TPP. Secondly, the C=O and NH₂ vibrations bands (1650 and 1584 cm^{-1} , respectively) are shifted to lower wavenumbers. Furthermore, the band at 1632 cm^{-1} is also broader which suggest different molecular environment in the DCsN structure due to intermolecular interactions.⁴⁰ Finally, the bands observed at 1218 cm^{-1} and 892 cm^{-1} in the DCsN spectra are attributed to P=O stretching vibration and P-O-P asymmetric stretching vibration, which also appear in the TPP spectrum, demonstrating its presence in the nanoparticles.⁴⁰

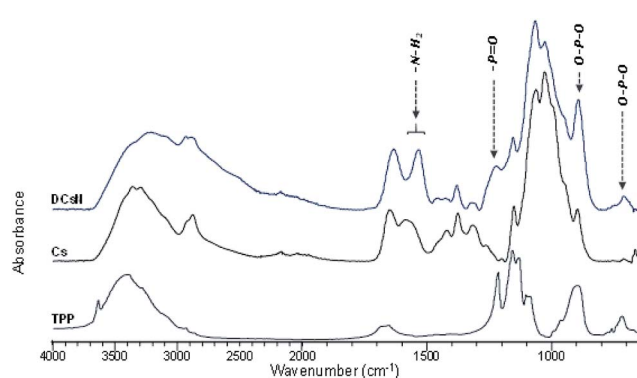


Fig. 4 ATR-FTIR spectra of DCsN, Cs, and TPP.

3.2.3. Thermal characterization. To determine the effect of the ionotropic gelation and scCO₂ drying on the thermal stability of the nanoparticles, thermogravimetric (TG) and differential thermogravimetric (DTG) curves of Cs and DCsN were obtained (Fig. 5). For Cs, three main steps are observed in the thermogram. The first step, attributed to the moisture evaporation, goes up to 130 °C and cause 7% of mass loss. The second step corresponds to the main phase of polymer degradation, with a highest rate close to 300 °C and 40% of weight loss associated. This phase includes the dehydration of the saccharide rings, thermal depolymerization and decomposition of the molecular units of Cs chain.⁴¹ Similar thermal behavior is typical for the degradation of Cs and other polysaccharides.^{40,42} The last step, related to secondary thermolysis processes, occurs over 400 °C leaving less than 10% of residual mass. Conversely, the first weight loss stage of DCsN is shorter than in Cs, which could be a consequence of less dense structure. Furthermore, the thermal degradation of DCsN starts at a lower temperature than in Cs. The higher stability of the untreated polysaccharide could be related to the presence of more microcrystalline domains that provides transitory stability at elevated temperature conditions. The residual mass after pyrolysis (char yield) for Cs and DCsN was 6 and 40% at 800 °C, respectively. Apparently, the presence of inorganic matter (e.g. TPP) affects the final outcome of the thermal reactions. In general, the processes involved to produce DCsN decrease to some extent the thermal stability of the polysaccharide and causes the start of disintegration at lower temperatures. Such difference could be associated with the higher relative rigidity of the internal structure in DCsN, due to multiple intermolecular interactions. The DSC curves (dash lines Fig. 5) of Cs and DCsN shows exothermic peaks centered at 331 °C and 238 °C, respectively. These peaks are related to the decomposition temperature of the polysaccharide, and their onset depends on the crystallinity, water content and acetylation degree of the Cs.⁴³ Congruently,

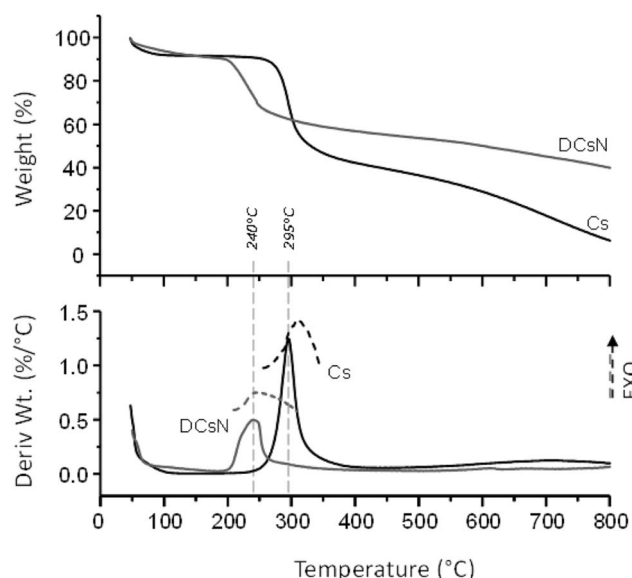


Fig. 5 TGA, DTG and DSC curves (dash lines) of Cs and DCsN.



both exothermic peaks correspond with the peaks of the DTG of Cs and the DCsN, reinforcing the arguments of thermal processes are affected mainly by crystallinity and crosslinking of the Cs molecules.

3.2.4. XRD. XRD analysis was carried out to determine the crystallinity of the materials and the results are shown in Fig. 6. Cs shows diffraction peaks at $2\theta = 9.8^\circ$ and 20° corresponding to the respective equatorial (020) and (110) of the microcrystalline reflections reported for Cs.⁴⁴ The main diffractive regions of the DCsN profiles were centered at 18° and 23° with notoriously lower intensity, indicating that DCsN is more amorphous than the pristine polymer, with almost no ordered structure. The crystallinity index for Cs and DCsN was 59.5% and 30.6% respectively. Similar results were reported for monoliths obtained from covalent gels dried with scCO₂.³¹

3.3. DCsN structural features

In order to shed light on the influence of scCO₂ drying on the morphology of the DCsN, a sample of lyophilized Cs nanoparticles (LCsN) was obtained from CsN. The freezing process was carried out as fast as possible, in liquid nitrogen, to induce the formation of smaller and uniform ice crystals. The lyophilization is the most used technique to obtain dry nanoparticles, mainly in order to facilitate their characterization and storage.⁴⁵

The specific surface area of the dry nanoparticles (DCsN and LCsN) was measured by N₂ sorption method using the BET (Brunauer–Emmett–Teller) model. In the adsorption isotherms (Fig. 7), it is possible to observe that DCsN display a type IV isotherm with hysteresis loop. This behavior has been associated with capillary condensation into mesopores and the limiting uptake over a range of high relative pressure.⁴⁶ Whereas, the LCsN produce a type II adsorption isotherm that is associated to macroporous materials.⁴⁶ Moreover, the DCsN have a specific surface area ($10.76 \text{ m}^2 \text{ g}^{-1}$) an order of magnitude higher than LCsN ($1.97 \text{ m}^2 \text{ g}^{-1}$).

These results indicate structural differences among DCsN and LCsN that could be attributed to changes induced by their respective drying procedures based in dissimilar principles. Lyophilization tends to modify previously formed structures, primarily due to ice crystals formation and solutes

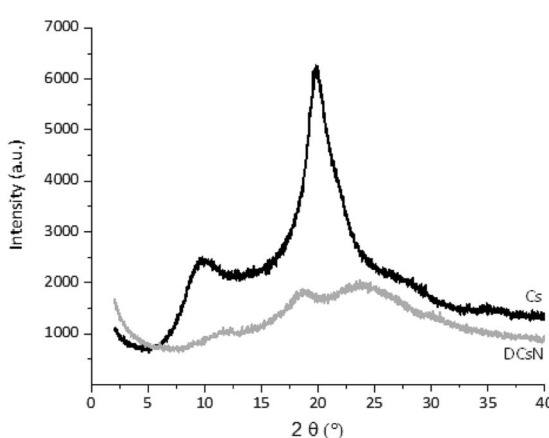


Fig. 6 XRD diffractograms of Cs and DCsN.

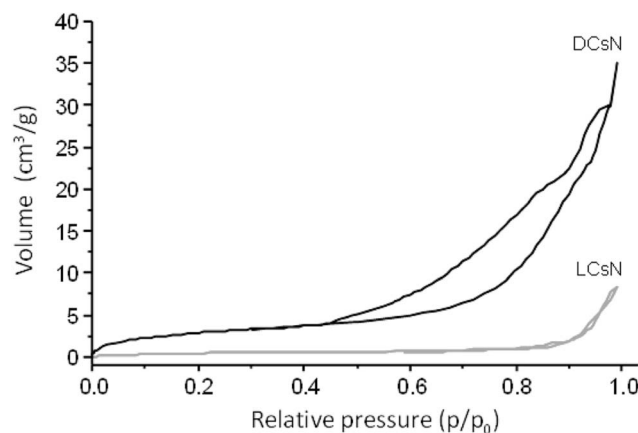


Fig. 7 N₂ adsorption–desorption isotherms of DCsN and LCsN.

concentration effects.⁴⁷ As consequence of the multiple disruptions caused by the high concentration of ice crystals in the suspension, there is considerable loss of the intrinsic structure of the gel nanoparticles. Usually, freeze-dried materials resemble macroscopic porous structures made of xerogel films. Alternatively, the scCO₂ drying technology is based on the replacement of the fluid phase of a colloidal system (e.g. a gel or particle suspensions) with CO₂ in conditions over its critical point, and then the pressure is reduced to release the CO₂ as a gas. Indeed, the network structure formed by the ionic gelation of Cs with TPP could be modified due to the successive replacement of liquid phase, from aqueous to ethanol, with different interaction with the polymer. However, at the drying stage, when the liquid phase (scCO₂) turns into gas, the surface tension is negligible minimizing the effects over previously formed network structure. The scCO₂ drying procedure reduces to a minimum the negative effects of surface tension over structural features normally producing mesoporous and low-density materials.^{48,49}

Some of the mentioned structural features could be observed in the FE-SEM images of the different dry nanoparticles (Fig. 8). At the higher magnification, it is possible to perceive that the DCsN (Fig. 8B) form a porous structure by aggregated individual nanoparticles. It would appear that the liquid phase replacement procedure cause particle aggregation. Similar structural features have been seen in scCO₂ dried materials from Cs chemical and physical gels.^{27,29} Also in agreement with the previous results, the LCsN materials appear to be made up by film-like structures forming macroporous scattered pieces (Fig. 8C and D).

3.4. Resuspension of DCsN

DCsN resuspension tests, in dilute acid (CH₃COOH 2% v/v) and pure water, were carried out to explore the functional behavior of the dry nanoparticles and envisage the possible applications of this material. When DCsN are mixed into acidic media, the particles were solvated, and an opalescent suspension was achieved. This indicates that the ionic crosslinks stand the acid conditions (pH \sim 4) hindering the Cs dissolution process. A



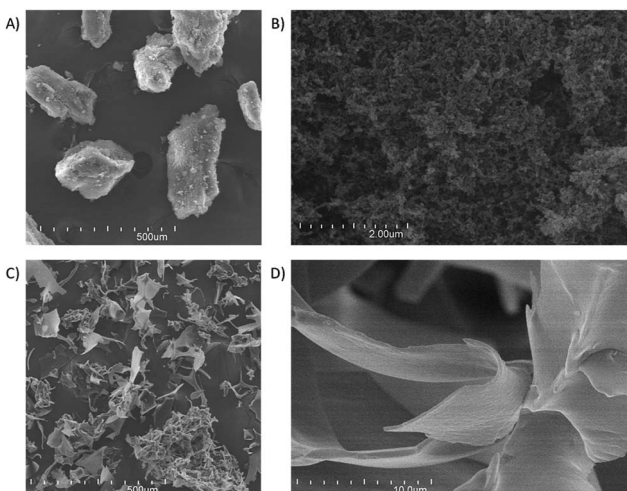


Fig. 8 FE-SEM images of: (A) DCsN at 100 \times magnification; (B) DCsN at 20 000 \times mag.; (C) LCsN at 100 \times mag.; (D) LCsN at 5 000 \times mag. All images were acquired with SE detector and 20.0 kV.

different outcome was observed in pure water where a considerable portion of the material remains aggregated. According to DLS measurements, the average hydrodynamic diameter of the resuspended DCsN in diluted acid was 149 ± 61 nm (PDI = 0.41) with a ζ -potential value of $+52 \pm 6$ mV. As ζ -potential values above +50 mV are associated to colloidal systems with good stability,⁵⁰ it is reasonable to expect that DCsN forms stable suspensions in slightly acidic aqueous media. Concerning to the increase of ζ -potential, compared with CsN, this may be due to molecular arrangements induced by the protonation of available amino groups of Cs chains in acidic medium. However, as can be observed in the FE-SEM image (Fig. 9) apparently the resuspended particles are formed by aggregated individual nanoparticles. The apparent diameter of the acid

resuspended DCsN was 73 ± 21 nm, measured from SEM images. Similar size reduction has been observed in other materials dried by scCO₂ treatment, mainly related to molecular interactions and rearrangements in the gels during the change of liquid phase.^{28,30} The aggregates of reduced size nanoparticles reach higher surface charge when are resuspended in an acidic media, however this charge is not enough to separate them completely.

4. Conclusions

Drying Cs nanoparticles by simple supercritical CO₂ drying procedure was possible. Initially, spherical Cs nanoparticles were produced by ionotropic gelation with an average of approximately 97 nm of hydrodynamic diameter and positive surface charge in water suspension. The proposed drying procedure includes a liquid phase replacement process (*i.e.* water to ethanol) that apparently generates particles aggregation. As a consequence a conglomerated porous structure is observed in the DCsN. The further structural analysis demonstrates that the scCO₂ drying produces materials with higher surface area compared with the lyophilized CsN. The physico-chemical characterization indicates that the scCO₂ drying does not affect the chemical structure of the polysaccharide and the thermal properties observed are related to the ionic cross-linking induced by the TPP. The DCsN were effectively dispersed in diluted acidic media resulting in stable colloidal suspension. These results open the possibility to produce dry chitosan nanomaterials with the extended surface area, porous structure and good resuspension capacity using an uncomplicated and environmentally safe scCO₂ drying technology. It is estimated that materials with such properties result appealing for diverse application. Studies to explore the possibilities to use DCsN type materials as bioactive compounds carriers are in progress.

Acknowledgements

The authors want acknowledge the financial support of CONACYT through the Project CB-2011-01-169626 and the fellowship DC2013-256 for JCL. Similarly it is recognized the valuable input of the technical staff of the Biopolymer Research Group of CIAD.

References

- 1 M. Rinaudo, *Prog. Polym. Sci.*, 2006, **31**, 603–632.
- 2 D. Bento, H. F. Staats, T. Gonçalves and O. Borges, *Eur. J. Pharm. Biopharm.*, 2015, **93**, 149–164.
- 3 S. Rodrigues, M. Dionísio, C. R. López and A. Grenha, *J. Funct. Biomater.*, 2012, **3**, 615–641.
- 4 Y. Zhou, S. Liu, H. Peng, L. Yu, B. He and Q. Zhao, *Int. Immunopharmacol.*, 2015, **28**, 34–43.
- 5 T. Kean and M. Thanou, *Adv. Drug Delivery Rev.*, 2010, **62**, 3–11.
- 6 J. Lizardi-Mendoza, W. M. Argüelles Monal and F. M. Goycoolea Valencia, in *Chitosan in the Preservation of*

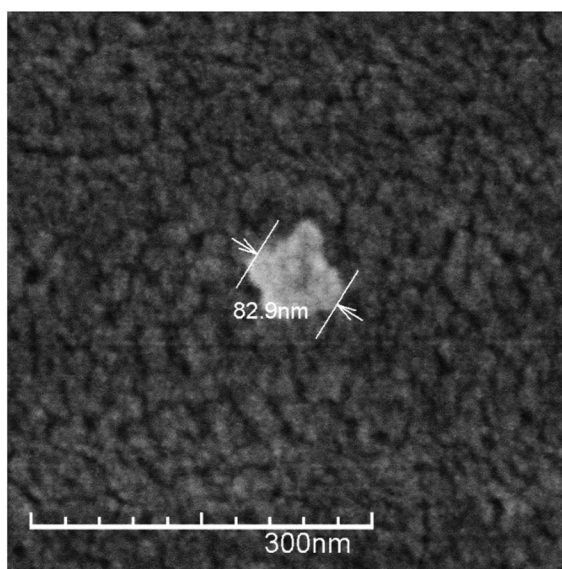


Fig. 9 FE-SEM image of a re-suspended DCsN particle. Magnification of 150 000 \times ; SE detector, 1.5 kV.



Agricultural Commodities, ed. Silvia Bautista-Baños, G. Romanazzi and A. Jiménez-Aparicio, Academic Press, San Diego, 2016, pp. 3–31.

7 C. K. S. Pillai, W. Paul and C. P. Sharma, *Prog. Polym. Sci.*, 2009, **34**, 641–678.

8 V. T. Tchemtchoua, G. Atanasova, A. Aqil, P. Filée, N. Garbacki, O. Vanhooteghem, C. Deroanne, A. Noël, C. Jérôme, B. Nusgens, Y. Poumay and A. Colige, *Biomacromolecules*, 2011, **12**, 3194–3204.

9 F. Croisier and C. Jérôme, *Eur. Polym. J.*, 2013, **49**, 780–792.

10 Z. Fülöp, P. Saokham and T. Loftsson, *Int. J. Pharm.*, 2014, **472**, 282–287.

11 V. Hamilton, Y. Yuan, D. A. Rigney, B. M. Chesnutt, A. D. Puckett, J. L. Ong, Y. Yang, W. O. Haggard, S. H. Elder and J. D. Bumgardner, *Polym. Int.*, 2007, **56**, 641–647.

12 K. Murakami, H. Aoki, S. Nakamura, S. Nakamura, M. Takikawa, H. Motoaki, S. Kishimoto, H. Hattori, Y. Tanaka, T. Kiyosawa, Y. Sato and M. Ishihara, *Biomaterials*, 2010, **31**, 83–90.

13 M. Garcia-Fuentes and M. J. Alonso, *J. Controlled Release*, 2012, **161**, 496–504.

14 A. Grenha, *J. Drug Targeting*, 2012, **20**, 291–300.

15 Y. Ohya, M. Shiratani, H. Kobayashi and T. Ouchi, *J. Macromol. Sci., Part A: Pure Appl. Chem.*, 1994, **31**, 629–642.

16 F. Sonvico, A. Cagnani, A. Rossi, S. Motta, M. T. Di Bari, F. Cavatorta, M. J. Alonso, A. Deriu and P. Colombo, *Int. J. Pharm.*, 2006, **324**, 67–73.

17 P. Calvo, C. Remuñán-López, J. L. Vila-Jato and M. J. Alonso, *J. Appl. Polym. Sci.*, 1997, **63**, 125–132.

18 H. Tokumitsu, H. Ichikawa and Y. Fukumori, *Pharm. Res.*, 1999, **16**, 1830–1835.

19 W. Abdelwahed, G. Degobert, S. Stainmesse and H. Fessi, *Adv. Drug Delivery Rev.*, 2006, **58**, 1688–1713.

20 A. Grenha, B. Seijo and C. Remuñán-López, *Eur. J. Pharm. Sci.*, 2005, **25**, 427–437.

21 L. T. K. Ngan, S.-L. Wang, D. M. Hiep, P. M. Luong, N. T. Vui, T. M. Dinh and N. A. Dzung, *Res. Chem. Intermed.*, 2014, **40**, 2165–2175.

22 P. Sheth, H. Sandhu, D. Singhal, W. Malick, N. Shah and M. S. Kislalioglu, *Curr. Drug Delivery*, 2012, **9**, 269–284.

23 N. Hijazi, E. Rodier, J.-J. Letourneau, H. Louati, M. Sauceau, N. Le Moigne, J.-C. Benezet and J. Fages, *J. Supercrit. Fluids*, 2014, **95**, 118–128.

24 S. M. Ghoreishi, A. Hedayati and M. Kordnejad, *J. Supercrit. Fluids*, 2016, **111**, 162–170.

25 H.-T. Wu, H.-K. Lee, H.-C. Chen and L.-J. Chien, *Chem. Eng. Res. Des.*, 2015, **104**, 615–625.

26 R. P. Cabral, A. M. L. Sousa, A. S. Silva, A. I. Paninho, M. Temtem, E. Costa, T. Casimiro and A. Aguiar-Ricardo, *J. Supercrit. Fluids*, 2016, **116**, 26–35.

27 H. Ennajih, R. Bouhfid, E. M. Essassi, M. Bousmina and A. El Kadib, *Microporous Mesoporous Mater.*, 2012, **152**, 208–213.

28 R. Valentin, B. Bonelli, E. Garrone, F. Di Renzo and F. Quignard, *Biomacromolecules*, 2007, **8**, 3646–3650.

29 X. Chang, D. Chen and X. Jiao, *J. Phys. Chem. B*, 2008, **112**, 7721–7725.

30 C. A. García-González, M. Alnaief and I. Smirnova, *Carbohydr. Polym.*, 2011, **86**, 1425–1438.

31 S. Takeshita and S. Yoda, *Chem. Mater.*, 2015, **27**, 7569–7572.

32 R. Zarzycki, Z. Modrzejewska, M. Dorabialska, G. Rogacki and A. Wojtasz-Pająk, *Drying Technol.*, 2009, **27**, 1370–1378.

33 F. M. Goycoolea, G. Lollo, C. Remuñán-López, F. Quaglia and M. J. Alonso, *Biomacromolecules*, 2009, **10**, 1736–1743.

34 A. B. Vishu Kumar, M. C. Varadaraj, R. G. Lalitha and R. N. Tharanathan, *Biochim. Biophys. Acta, Gen. Subj.*, 2004, **1670**, 137–146.

35 H. Zhang, Q. Huang, Z. Huang, T. Liu and Y. Li, *Int. J. Pharm.*, 2015, **479**, 212–218.

36 Q. Gan, T. Wang, C. Cochrane and P. McCarron, *Colloids Surf., B*, 2005, **44**, 65–73.

37 H. Saito, R. Tabeta and K. Ogawa, *Macromolecules*, 1987, **20**, 2424–2430.

38 K. Ogawa, T. Yui and K. Okuyama, *Int. J. Biol. Macromol.*, 2004, **34**, 1–8.

39 J. Brugnerotto, J. Lizardi, F. M. Goycoolea, W. Argüelles-Monal, J. Desbrieres and M. Rinaudo, *Polymer*, 2001, **42**, 3569–3580.

40 S. Walke, G. Srivastava, M. Nikalje, J. Doshi, R. Kumar, S. Ravetkar and P. Doshi, *Carbohydr. Polym.*, 2015, **128**, 188–198.

41 C. Peniche-Covas, W. Argüelles-Monal and J. San Román, *Polym. Degrad. Stab.*, 1993, **39**, 21–28.

42 D. Fernández-Quiroz, Á. González-Gómez, J. Lizardi-Mendoza, B. Vázquez-Lasa, F. M. Goycoolea, J. San Román and W. M. Argüelles-Monal, *Carbohydr. Polym.*, 2015, **134**, 92–101.

43 L. S. Guinesi and E. T. Gomes Cavalheiro, *Carbohydr. Polym.*, 2006, **65**, 557–561.

44 Y. Zhang, C. Xue, Y. Xue, R. Gao and X. Zhang, *Carbohydr. Res.*, 2005, **340**, 1914–1917.

45 P. Fonte, S. Reis and B. Sarmento, *J. Controlled Release*, 2016, **225**, 75–86.

46 K. S. W. Sing, *Pure Appl. Chem.*, 2009, **57**, 603–619.

47 F. Franks, *Eur. J. Pharm. Biopharm.*, 1998, **45**, 221–229.

48 M. Alshrah, M.-P. Tran, P. Gong, H. E. Naguib and C. B. Park, *J. Colloid Interface Sci.*, 2017, **485**, 65–74.

49 R. Valentin, K. Molvinger, F. Quignard and D. Brunel, *New J. Chem.*, 2003, **27**, 1690–1692.

50 S. Bhattacharjee, *J. Controlled Release*, 2016, **235**, 337–351.

